Frequency dynamics of the Northern European AC/DC power system: a look-ahead study

Danilo Obradović, *Student Member, IEEE,* Matas Dijokas, *Student Member, IEEE,* Georgios Misyris, *Student Member, IEEE,* Tilman Weckesser, *Senior Member, IEEE,* and Thierry Van Cutsem, *Fellow, IEEE*

***Abstract*—In many power systems, the increased penetration of inverter-based renewable generation will cause a decrease in kinetic energy storage, leading to higher frequency excursions after a power disturbance. This is the case of the future Nordic Power System (NPS). The look-ahead study reported in this paper shows that the chosen units participating in Frequency Containment Reserves (FCR) cannot keep the frequency above the prescribed threshold following the outage of the largest plant. This analysis relies on a detailed model of the Northern European grid. The latter is compared to the classical single-mass equivalent, and the impact of voltage-dependent loads is assessed in some detail. Next, the paper focuses on emergency power control of the HVDC links that connect the NPS to the rest of the European grid, which can supplement or even replace part of the FCR. The proper tuning of that control is discussed. Finally, the analysis is extended to the HVDC links connecting the future North Sea Wind Power Hub under two configurations, namely low and zero inertia. The impact of outages in the latter sub-system is also assessed. The material to simulate the system with industrial software is made publicly available.**

***Index Terms*—Frequency Containment Reserves, HVDC frequency support, Nordic Power System, North Sea Wind Power Hub.**

I. Introduction

THE continuous drive to reduce carbon emissions and meet the climate agreement goals is reshaping power systems all over the world. Amongst many factors, the large-scale integration of inverter-based generation and the increasing interconnection capacity, contribute the most in phasing out conventional power plants, thereby decreasing power system kinetic energy storage. With lower inertia, the frequency response to power imbalances worsens, challenging Transmission System Operators (TSOs) to securely operate power systems [1]. The problem has already been observed in island systems, e.g. Ireland or Australia [2], [3], and it is progressively affecting larger interconnected systems as well, such as Great Britain (GB).

This holds true also in the Nordic countries (Norway, Sweden, Finland, and Denmark) [4], [5]. The Nordic Power System (NPS) is shown with dark blue color in Fig. 1. This system has experienced a progressive growth of wind generation with a cumulative power almost doubled over the past 10 years [6] and the forecast shows that capacity is expected to double again by 2030 [7]. In parallel, global policies to reinforce the interconnected European grid and increase generation from renewable energy sources [8] are already taking effect with an additional 4.9 GW of new interconnection capacity scheduled to be operational by 2025 (see dashed lines in Fig. 1) [5]. As a result, by 2040, the total kinetic energy of synchronous generators in the NPS may drop below 125 GWs for more than 2100 hours per year, while this lower limit is very seldom reached nowadays [9]. Several reports have already addressed the decreasing kinetic energy issue in the NPS [5], [10], [11]. The most noticeable consequence is in case of a large disturbance a drop of the system frequency below the threshold value of 49.0 Hz imposed to leave a security margin with respect to the settings of underfrequency load shedding protections. The current

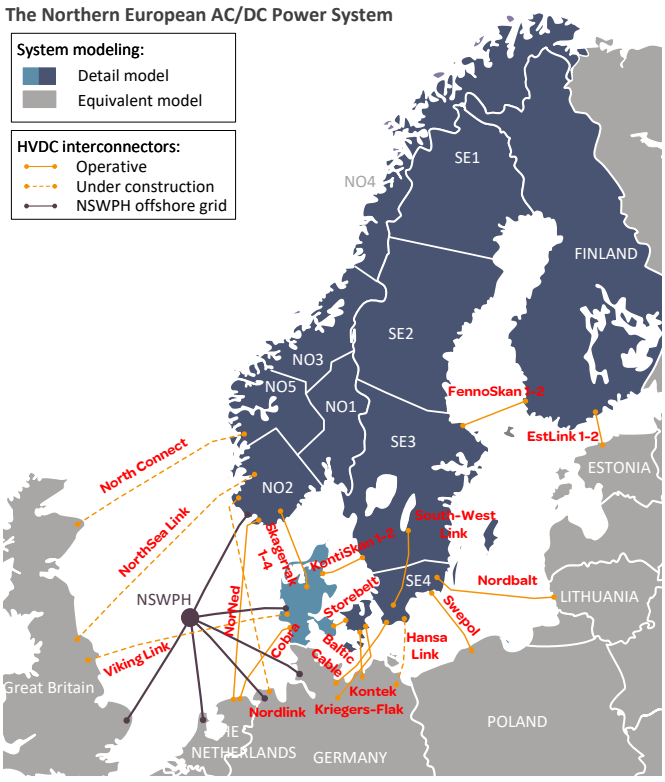

Fig. 1. Northern Europe, North Sea Wind Power Hub and HVDC interconnectors. The model presented in the paper is shown in blue. The dark blue part corresponds to the Nordic Power System. Numbers appearing in line names correspond to multiple HVDC line in parallel.

D. Obradović is with KTH Royal Institute of Technology, Stockholm, Sweden (e-mail: daniloo@kth.se). M. Dijokas and G. Misyris were, and T. Weckesser is with Technical University of Denmark, Department of Electrical Engineering, Kgs. Lyngby, Denmark (emails: matdij, gmisy, tweck@elektro.dtu.dk). T. Van Cutsem was with the Fund for Scientific Research (FNRS) at the Dept. of Electrical Engineering and Computer Science, University of Liège, Belgium (e-mail: t.vancutsem@uliege.be).

This work is supported by the multiDC project, funded by Innovation Fund Denmark, Grant Agreement No. 6154-00020B.

Frequency Containment Reserve (FCR) (or primary frequency control reserve) requirements are not likely to be sufficient to contain frequency deviations above the prescribed limit, following the dimensioning incident, which is the outage of the largest unit, namely the 1450-MW Oskarshamn-3 nuclear power plant located in Sweden [12]. One option would be to decrease the severity of the dimensioning incident by reducing the production of that nuclear power plant and compensating on other units. This solution, however, is not attractive from a market viewpoint. The same holds true for the participation of more units in FCR. Other frequency control means are thus needed [13].

In this respect, a distinctive feature of the NPS is the large number of HVDC links through which it is already connected to Continental Europe (CE), as depicted in Fig. 1. This figure also shows the additional links that will be available in the future. Currently, these links are equipped with step-based Emergency Power Control (EPC) as defined in [10]. However, due to poor coordination for various disturbances and potential stability issues in low inertia conditions [14], the change of control paradigm to droop frequency-based EPC is contemplated for near-future operation [15]. In this respect, Ref. [15] suggests the reserve amounts and activation thresholds for the NPS, CE, and GB. However, the exact values of gains and their distribution have not been discussed.

The literature proposes various ways to support the frequency of AC systems such as wind power-HVDC systems [16]- [18], multi-terminal HVDC grids [19]- [21], and fast frequency reserve sources [22], [23]. Furthermore, assuming advanced communication infrastructure and adaptive control capabilities, interesting control methods were assessed in [24]-[27]. However, in accordion with [15], TSOs must favor robustness and security of HVDC frequency support over optimality. This makes the "simpler" droop frequency-based EPC more attractive. With this technique, when activated, EPC output is always proportional to frequency deviation, which enables a high level of EPC controllability. Even more, it has been shown that this type of control improves small-signal stability of the AC system [28], [29].

Another opportunity for NPS frequency control is the future availability of the North Sea Wind Power Hub (NSWPH), in the form of a cluster of artificial islands connected to onshore grids though multiple point-to-point HVDC links. Its first objective is to harvest a large amount of wind energy. The North Sea potentially offers as much as 36 GW of wind power collectable through such a cluster of islands [30]. The second objective is to use the NSWPH as a hub for power exchanges among partner TSOs, as illustrated in Fig. 1, allowing in particular the frequency of one system to be supported by other, asynchronous systems. To that purpose, the mechanism of EPC can be applied to the HVDC links connecting the hub. Reference [31] has already presented a scaled-down version with a single island and has assessed the stability of this isolated AC system, asynchronous with the onshore grids.

Frequency dynamics are very often studied using the so-called single-mass simplified model in which all plants of the same type (e.g. hydro, thermal, etc.) are aggregated and represented through equivalent turbines and individual loads lumped into a single equivalent load. This model, however, does not account for the voltage dependency of load powers. Under the effect of the initial disturbance, the various voltages undergo variations, even more in parts of the system depleted with synchronous machines and not reinforced by equivalent voltage controlling devices. Those voltage variations affect the load powers, which in turn impacts frequency dynamics. The opposite trend can be observed where HVDC links using Voltage Source Converters (VSC) participate in grid voltage control.

In the context of the multiDC project (see www.multi-dc.eu) a detailed model of the Nordic and Western Danish systems, shown respectively in dark and light blue in Fig. 1, has been set up, which preserves the topology of the grid. The frequency response of this model was found to differ from that of the corresponding single-mass equivalent. Those discrepancies are assessed in some detail in this paper. Furthermore, the detailed model takes into account the local impacts of HVDC links and considers the tuning of their individual contributions to EPC.

The overall purpose of this paper is not to propose new controls or new models. Rather, it aims at documenting a study of the future NPS frequency dynamics in the context of strategic system changes foreseen for the period 2020-2030, with emphasis on HVDC support complementing and/or replacing FCR in operating conditions with low kinetic energy storage.

More specifically, the contributions of the paper are:

- a look-ahead study of the frequency dynamics of the NPS, as an example of large-scale system exposed to a significant reduction of its kinetic energy storage;
- the outline of a detailed NPS multimachine model (under the phasor approximation) including individual (operational and planned) point-to-point HVDC links with Line Commutated Converters (LCC) and VSC (the former with their slower-acting reactive power compensation), wind parks under voltage or reactive power control and voltage dependent loads;
- a comparison between the detailed and the single-mass models showing the impact of network voltages variations on frequency transients;
- an evaluation of the benefits of EPC on frequency dynamics from steady-state and dynamic viewpoints, including the replacement of FCR provided by the (hydro) power plants;
- a discussion of the proprer tuning of EPC acting on individual links;
- the extension of this analysis to future HVDC links connecting the NSWPH to onshore grids and exploiting the onshore frequency deviation signals to control the offshore AC/DC converters;
- conversely, examples of how outages in the NSWPH system itself impact the onshore grids under two options, namely low- or zero-inertia.

The detailed model involves generic, non-proprietary models. The corresponding material can be publicly accessed and used by other researchers.

The rest of the paper is organized as follows. An overview of the NPS and its model is given in Section II. Sections III

and IV present the salient features of the system: NSWPH and HVDC EPC, respectively. Dynamic simulation results are provided and discussed in Section V. Concluding remarks are offered in Section VI.

II. The Northern European system and its model

A. Frequency control in the NPS

The NPS makes up one synchronous area with a nominal frequency of 50 Hz. It is operated by four TSOs. The total load ranges from 25 to 70 GW, while the total kinetic energy of synchronous generators varies in between 110 and 240 GWs at the moment. Currently, the grid is connected to the rest of Northern Europe through 18 point-to-point HVDC links and five more are being developed (see Fig. 1) [10].

Frequency regulation resorts to the following main services: FCR for Normal operation (FCR-N), FCR for Disturbances (FCR-D) and Frequency Restoration Reserve (FRR). In normal system operation the frequency deviations are limited to $\pm$100 mHz and FCR-N is deployed to keep the frequency inside that standard band. In case of a larger power imbalance, when frequency drops below 49.9 Hz, FCR-D is activated. FRR is used to restore the frequency back to nominal value. The system is designed to operate with a system stiffness [32] of at least 3625 MW/Hz with the objective of limiting the steady-state frequency deviation to $\pm$ 500 mHz [33].

The maximum Instantaneous Frequency Deviation (IFD) must be smaller than $\pm$1 Hz. Under-frequency load shedding is activated at 48.8 Hz. Although its activation is deemed unlikely (only for a large disturbance, low inertia, and poor FCR performance), it would lead to a heavy compensation cost. Therefore, the NPS TSOs have set the lowest allowed frequency to 49.0 Hz and they have accordingly determined actions to decrease the risk of load shedding activation.

B. Overview of the model

The developed model, corresponding to the blue areas in Fig. 1, includes the following:

- Norway (NO), Sweden (SE) and Finland (FI) represented only with their extra-high-voltage transmission network (300 and 400 kV), which includes a large number of long transmission lines;
- The eastern part of Denmark (DK2), which belongs to the same synchronous (NPS) zone. Owing to the large number of HVDC links connected to Denmark, it was decided to represent the Danish grid in greater detail, down to lower voltage levels (400, 165 and 150 kV). This involves much shorter lines/cables and a comparatively large number of substations;
- The western part of Denmark (DK1), which is synchronous with CE. For the same reason as above, that part of the Danish grid involves lower voltage levels.

The main characteristics of the model are listed in Table I.

TABLE I
Summary of the main model characteristics

	Nordic Power System				DK1
	NO	SE	FI	DK2	
# of buses	45	30	13	140	171
# of transmission lines	35	27	5	174	165
# of generators	16	9	5	17	29
# of WPPs	4	6	2	17	35
# of loads (neg. loads)	15	13	9	139(73)	135(99)
# of compensation units	2	3	-	21	62
Total generation [MW]	43723				2113
Total load [MW]	43531				2936
# of HVDC lines	24				

At the other end of HVDC links, the neighbouring synchronous zones, in particular GB and CE, are represented with single-mass equivalents and simplified frequency control.

The model takes into account the strategic changes identified in [5]: increased wind power production, decommissioning of nuclear power plants, internal grid reinforcements and new interconnections.

The focus of the study is on frequency and long-term dynamics (lasting up to - say - one minute after a disturbance), which led to represent slow controls such as Load Tap Changers and shunt compensation switching. The model has been developed under the phasor approximation [32]. The DigSilent PowerFactory 2018 software has been used to that purpose [34]. Since all components are represented by generic models and no proprietary information is involved, the data have been made publicly available and can be accessed at [35].

The generation mix is dominated by hydro and thermal power plants. In total, 76 generation units with nominal power above 40 MVA are represented behind their step-up transformers. All synchronous machines have a 5^{th} or 6^{th} order model (equivalent to model 2.1 and 2.2 according to [36]), including saturation effects, supplemented with automatic voltage regulator and Power System Stabilizer (PSS) models. The latter were tuned to ensure a sufficient level of rotor angle stability. The generators below 40 MVA were represented as negative loads.

Ten generators participate in FCR-D and these are driven by hydro turbine/governor models. The corresponding parameters were selected in realistic ranges of values, and using the methodology in [14] to satisfy the existing requirements for FCR-D.

The consumption is represented as aggregated loads at specific voltage levels. The dependency of load power to voltage is represented with a ZIP model [32]. Its parameters were adopted from [37], in which loads were aggregated by type in each country and the model was validated against post-event measurements. No frequency dependency of loads has been considered, which is a little pessimistic.

The model includes 24 HVDC links, of which 13 involve AC/DC converters of the LCC type and 11 of the VSC type. Each LCC-HVDC link is modeled as a two-port element containing a DC cable, a rectifier and an inverter. The converters and their controls have generic models according to [38]. Each LCC converter station includes a transformer with load tap changer and switchable shunt capacitor banks. The transformer ratios and the shunt susceptances are adjusted by "slow", discrete controllers. Each VSC-HVDC link is modeled by a two-port element containing a DC cable, two converters, DC capacitors and phase reactors. The converters, based on

the Multimodular Multilevel Converter (MMC) technology [39], are equipped with grid-following Synchronous Reference Frame (SRF) controls, as presented in [31]. The controllers were carefully tuned to exhibit adequate dynamics. For instance, the response time after a step change of active power reference is within 200 ms for LCC links and 100 ms for VSC links. Most of the HVDC links operate in active power control mode, while VSCs are set to regulate the voltage at their points of connection behind a phase reactor.

Finally, the Wind Power Parks (WPP) are represented with grid-following SRF control including only the outer control loops (thus neglecting inner loops). The model does not consider any plant level control and assumes operation for maximum power point tracking.

C. System operating point

The majority of the power is provided by plants located along the Norwegian Coast and in Northern Sweden (see NO3, NO4, NO5, SE1, and SE2 zones in Fig. 1). The power is transferred along a North-South axis to meet high load demand in densely populated areas (see NO1, NO2, SE3, SE4, and FI zones in Fig. 1). The total load in NPS is 43.5 GW, of which 14.9 GW are covered by WPPs. The kinetic energy storage of the NPS system is around the low value of 125 GWs. The operating point was adjusted according to the commonly observed power flow orientations in HVDC interconnections and load centers, so that a plausible scenario for the future system is considered.

III. The North Sea Wind Power Hub and its Model

The NSWPH considered in the study would be located as shown in Fig. 2. Among many topologies, the AC hub emerges as a possible technical solution to accommodate and connect electrical equipment. The topology considered in this study consists of three identical islands connected through 400-kV submarine AC cables. The Hub-and-Spoke design, currently considered by the involved TSOs [40], allows modular expansion as well as isolation of an island in disturbed operation conditions.

The total installed capacity of the offshore WPPs connected to the NSWPH is 9 GW, each island harvesting 3 GW of wind generation. As shown in Fig. 3, in the model, the WPPs connected to each island are lumped into five equivalent WPPs, connected to a 400-kV local hub through 66-kV cables. Each equivalent WPP collects the same power but the length of the 66-kV connection varies from one WPP to another to account for their positions around the island. Six 2-GW ±525-kV VSC-HVDC links, two per island, connect the NSWPH to three onshore synchronous zones, namely GB, CE and NPS. The VSCs are based on the MMC technology [39]. The WPPs are operated in constant PQ mode with only the DC/AC converter dynamics represented; hence, they do not contribute to frequency or voltage control. This assumption was make to check the stability of the NSWPH in severe conditions.

Two control configurations have been contemplated, referred to as zero- and low-inertia.

In the low-inertia approach [31], [41], each AC island is equipped with a Synchronous Condenser (SC), as shown in Fig. 3. The frequency in the AC islands is set by the SC rotor speeds. Their kinetic energy storage allows smoothing the impact of offshore disturbances on onshore grids. The SCs, equipped with automatic voltage regulators, not only control the grid voltages but also provide a reference with which the VSCs synchronize. Hence, in this approach, each VSC can operate in grid-following mode, tracking the grid voltage phasor with a phase-locked loop and adjusting the phasor of its injected current in accordance with the desired active and reactive powers. Through the outer control loop shown in Fig. 4a, each VSC imposes an active power-frequency droop. The frequency deviation is slowly corrected by a hub coordinator with integral action on the frequency error as shown in Fig. 4b. It can also redistribute the power changes among the various VSCs according to participation factors. The nominal power of each SC is 300 MVA, a value that preserves stability of the NSWPH grid after the outage of any of the three SCs. The inertia constant H has been set to the average value of 5 s.

Zero-inertia refers to the absence of any rotating machine, i.e. it is a 100% converter-based system [31], [42]. Hence,

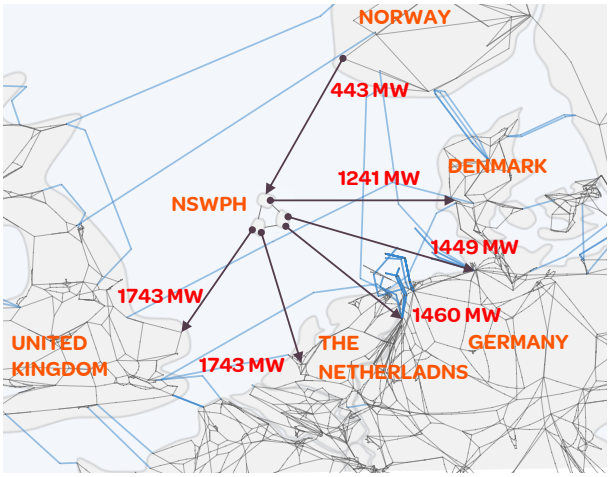

Fig. 2. Overview of three-island NSWPH topology with point-to-point HVDC connections to the onshore grids. The 400-kV transmission lines in the onshore grids are shown with thin black lines.

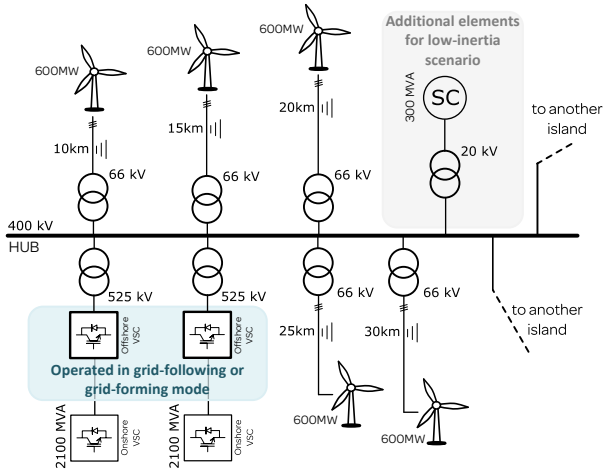

Fig. 3. AC grid topology in one of the NSWPH islands (low- and zero-inertia configurations)

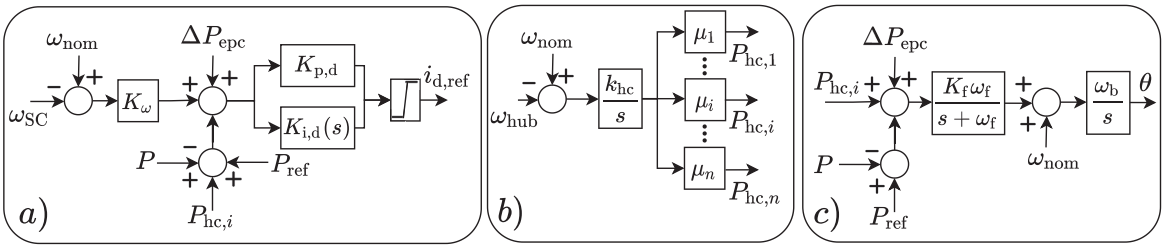

Fig. 4. Outer control loop block diagrams of the offshore VSCs: (a) grid-following control; (b) hub coordinator; (c) grid-forming control [43].

the offshore VSCs operate in grid-forming mode. Each VSC imposes the magnitude and phase angle of its modulated AC voltage, behind its step-up transformer. The various VSCs synchronize with each other through their individual control loops adjusting the frequency of each modulated voltage based on the difference between the measured active power and its set-point, according to the droop $K_{\rm f}$, as shown in Fig. 4c. The zero-inertia configuration allows keeping the NSWPH frequency close to its nominal value (50 Hz) and saves the footprint of the SCs. On the other hand, offshore power imbalances are quickly propagated to the DC voltages of the HVDC links and to the onshore grids. After a large disturbance any over-current in a grid-forming VSC is promptly corrected to avoid damage [44].

The links connected to GB and CE export power from the hub. Fig. 2 shows the power flows at the initial operating point. They would correspond to a common situation where Norway exports power [45], in this case 443 MW to the NSWPH.

IV. Emergency Power Control of HVDC links

The HVDC EPC aims to aid the conventional units involved in FCR-D to limit the IFD, namely to keep frequency above 49.0 Hz after the dimensioning incident. This emergency control relies on a corrective signal sent to the active power controllers of designated AC/DC converters to promptly increase or decrease the active power injection into the NPS. EPC relies on a closed-loop design, as shown in Fig. 5, in which the active power correction is proportional to the frequency deviation obtained from local measurement. More precisely, EPC is activated when the input frequency signal f reaches the triggering threshold f_h, after which the active power reference is adjusted by $\Delta P_{\rm epc}$ proportionally to the frequency error $f-f_h$. When the frequency signal regains a value above f_h, the active power reference $\Delta P_{\rm epc}$ is reset to zero, disabling the EPC correction of the converters.

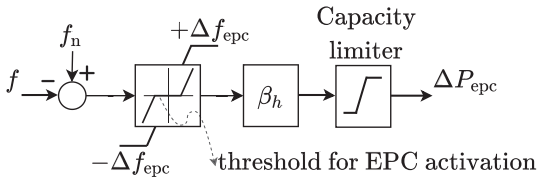

Fig. 5. Droop frequency-based HVDC EPC control block

All HVDC interconnections presented in Fig. 1 are involved in EPC with equal gains expressed on the MW base power of each link. The activation time delays are assumed negligible since local measurements are used, and the activation threshold f_h has been set to a different value from the FCR activation threshold f_g.

The procedure for EPC tuning consists of correctly determining total EPC gain. That (total) gain is distributed among various HVDC links that have available EPC headroom with equal per unit gains. This is performed in the worst scenario, i.e. after the dimensioning incident and for the lowest estimated kinetic energy value.

The primary purpose of EPC is to limit the maximum IFD, but additionally, EPC could support the system in steady-state, thereby providing TSOs with another degree of freedom to distribute post-disturbance powers and organize frequency reserves more efficiently. To this purpose, the following procedure is followed.

1) First, the FRC requirements are defined. This work follows the requirements and design specified in [46], which make reference to a single governor-turbine equivalent. The corresponding performances are matched and distributed over the various plants of the detailed model. The corresponding total steady-state FCR gain is β_{g0}, as defined in the Appendix, see Eq. (A.3). Even though various sets of dynamics governor parameters could fulfill the FCR requirements, in the context of the worst-case scenario, the selected ones relate to the maximum frequency deviation [14].
2) Once the FCR units have been defined, the total needed EPC gain β_{h0} (defined in (A.4) and (A.5)) is determined by the condition (A.6) in the Appendix A. It yields the maximum allowed IFD. This value is obtained iteratively by performing dynamic simulations.
3) From here, further increase of EPC gains will decrease both the IFD and the Steady-State Frequency Deviation (SSFD), but clearly this will come at the cost of increasing the EPC reserves. Therefore, a trade-off is achieved by replacing a part $\Delta\beta_g$ of the FCR reserves with EPC $\Delta\beta_h$ under the constraint of keeping the SSFD below the maximum allowed value. Assuming that the exchange of FCR and EPC reserves will not change the load nor the losses contribution to SSFD, $\Delta\beta_h$ is related to $\Delta\beta_g$ through:

$$\Delta\beta_h = \frac{\Delta f_{ss,g}}{\Delta f_{ss,h}}\Delta\beta_g, \tag{1}$$

where $\Delta f_{ss,g}$ and $\Delta f_{ss,h}$ represent the respective contributions of FCR and EPC to SSFD. In this way, the slow (and non phase-minimum in case of hydro turbines) FCR dynamics are replaced by fast EPC, which improves the

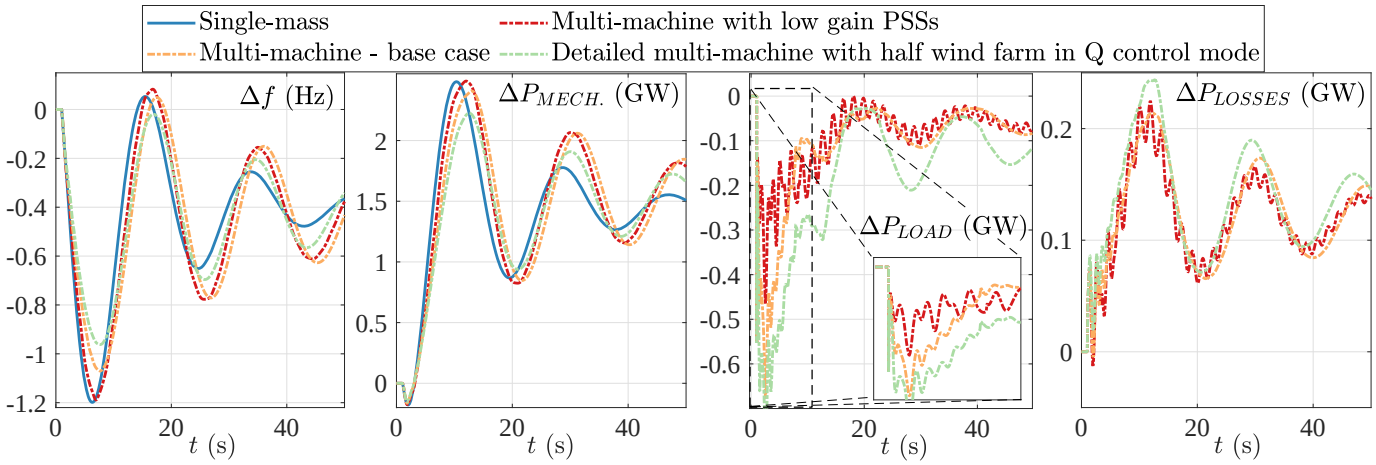

Fig. 6. System responses to the dimensioning incident for various models and voltage control assumptions.

IFD, with less increase of total reserves. FCR reserves being related to SSFD, and EPC to IFD, considering Eq. (1), the total reserves are given by:

$$P_{res} = \underbrace{\Delta f_{ss,g}(\beta_{g0} - \Delta\beta_g)}_{\text{FCR}} + \underbrace{\Delta f_{\text{ifd},h}(\beta_{h0} + \frac{\Delta f_{ss,g}}{\Delta f_{ss,h}}\Delta\beta_g)}_{\text{EPC reserves}} \quad (2)$$

where $\Delta f_{\text{ifd},h}$ is the new maximum IFD (lower than the maximum allowed). The latter has to be determined through dynamic simulations.

V. Simulation Results

The simulation results presented in this section deal with the frequency dynamics of the future Northern European AC/DC system, including the NPS and the NSWPH, without and with EPC, respectively. The simulations involve large disturbances such as a generator or HVDC interconnector outages. In all simulations, the system is initially in steady-state with the NPS frequency at 49.9 Hz (the lowest value with FCR-D reserves not activated) and the NSWPH frequency at 50 Hz.

The rest of this section is organized as follows. First, the use of a detailed model is motivated and the importance of including voltage dynamics is illustrated. Next, EPC is introduced and its design is presented with the aim of efficiently using the reserves. Finally, the contribution of the NSWPH to frequency support is considered, but also the possible impact of disturbances occurring in that isolated sub-system.

A. NPS frequency dynamics with FCR from generators

First, the system response to the dimensioning incident is considered. This involves the outage of the Oskarshamn-3 1450-MW nuclear power plant, located in zone SE3 (see Fig. 1). That response is studied with four different system models:

1) the detailed multi-machine model presented in Section II;
2) a single-mass equivalent model that has the same FCR and inertia characteristics as the detailed model;
3) a variant of the detailed model with reduced PSS gains;
4) another variant of the detailed model with half of the wind farms controlling their reactive powers instead of the AC voltages.

Figure 6 presents the corresponding simulation results. From left to right, the plots show the average frequency deviations, the total mechanical powers, the total load active powers, and the total active power losses. It can be seen that the lowest IFD is significantly different depending on the model. That difference is mainly explained by the variations in load and losses. In particular, the initial load decrease has a positive effect on the frequency deviation. This load reduction originates from the bus voltage magnitudes that drop across the system under the effect of the disturbance (especially near the location of the latter). The variant with lower PSS gains exhibits more tightly controlled generator voltages and hence the effect of voltage on load powers is less pronounced, thus yielding a significantly larger frequency excursion. On the other hand, when some wind farms converters are changed from voltage to reactive power control, larger voltage drops (and, hence, a larger load power decrease) are experienced, and the frequency deviation is smaller. All these results motivate to consider individual loads, and pay attention to generators and converters voltage/reactive power control.

On the other hand, Fig. 6 indicates that losses increase after the disturbance, which contributes to increasing the frequency deviation. That increase is explained by the larger power flow through an already stressed corridor that transfers power from north (where most of the FCR units are located) to south. No general conclusion can be drawn from this observation, and the trend could be different for a different initial power flow. However, the shown scenario is typical for the NPS.

Note that the mechanical power exhibits the well-known non phase-minimum behaviour of hydro turbines as well as the slow response rate of the associated FCR units, largely responsible for the inability to keep frequency above the prescribed threshold value.

Next, the system responses to various disturbances differing by their size and their location are considered. This allows to further assess the impact on frequency of voltage-dependent

TABLE II
LIST OF APPLIED GENERATORS TRIPS WITH THEIR LOCATION AND THE AMOUNT OF LOST POWER AND KINETIC ENERGY.

Disturbance	1	2	3	4	5	6	7	8	9	10	11	12
Zone	se3_a	fi1	no5	no2_b	no4	se3_b	no1_b	no1_a	se2	se4	no2_a	dk2
Power of outaged generator (GW)	1.45	1.16	1.07	1.05	1.04	1.02	0.97	0.90	0.80	0.79	0.67	0.30
Kinetic energy of outaged generator (GWs)	6.57	4.47	4.2	3.72	3.85	4.55	3.45	5.2	3.14	4.55	2.38	1.7

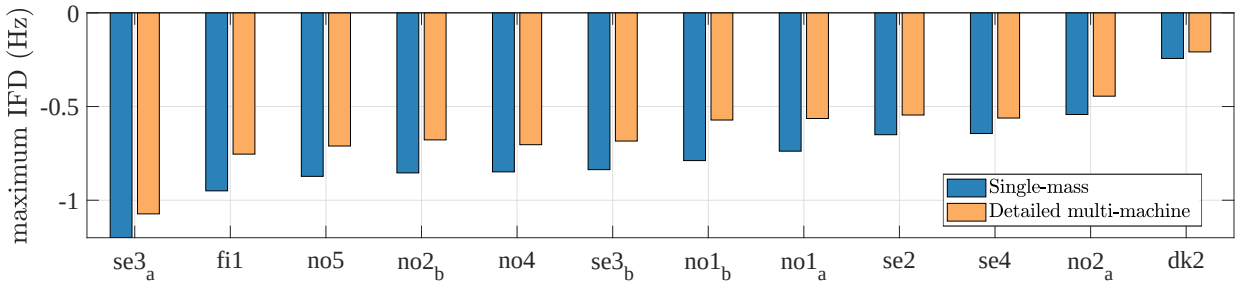

Fig. 7. Maximum frequency deviations for various disturbances; comparison between single-mass and detailed multi-machine models.

loads as well as the proximity of the disturbance to load centers. Although these effects are sometimes disregarded, they may be significant for proper design of frequency reserves in low-inertia systems.

The set of additional 11 disturbances detailed in Table II has been considered. The responses given by respectively the single-mass and the detailed multi-machine model are compared in Fig. 7 in terms of maximum IFD. It can be seen that the load dependency on voltage shows its effect to various extents, depending on the location of the disturbance. The way a given disturbance impacts IFD is a complex function of the whole system design. Nevertheless, the figure shows that the single-mass model, which does not account for the voltage dynamics, gives consistently a more pessimistic value of the maximum IFD.

B. NPS frequency dynamics with EPC

Figure 6 shows that, if the current frequency control requirements are kept unchanged in the time horizon of this study, the FCR units with a gain β_{g0} of $3,648$ MW/Hz will be unable to contain the IFD within the defined margin after the dimensioning incident. The results of this section show how EPC combined with FCR can efficiently contribute to frequency control in terms of maximum IFD and SSFD values.

As explained in Section IV, first, the total EPC gain β_{h0} is identified using dynamic simulations, in order to reach the maximum allowed IFD. This total EPC gain is then distributed over the 19 HVDC links so that the individual per-unit EPC gains are all equal. Furthermore, additional coordination between FCR units and EPC is sought in order to reduce the maximum IFD and decrease the total usage of reserves.

The corresponding results are provided in Fig. 8 showing, on the left, the frequency response and, on the right, the mechanical and the EPC powers. The results shown have been obtained with the following three control methods:

- FCR from hydro units only (as in Section V-A);
- EPC in addition to FCR units. The activation threshold has been set to 49.6 Hz. The maximum IFD is brought back to the allowed limit for a total EPC gain of 622 MW/Hz.
- Additional FCR reserves replaced by EPC according to Eq. (1) with $\Delta\beta_g = 1230$ MW/Hz which results in a new total EPC gain of 5542 MW/Hz ($\beta_{h0} + \Delta\beta_h$).

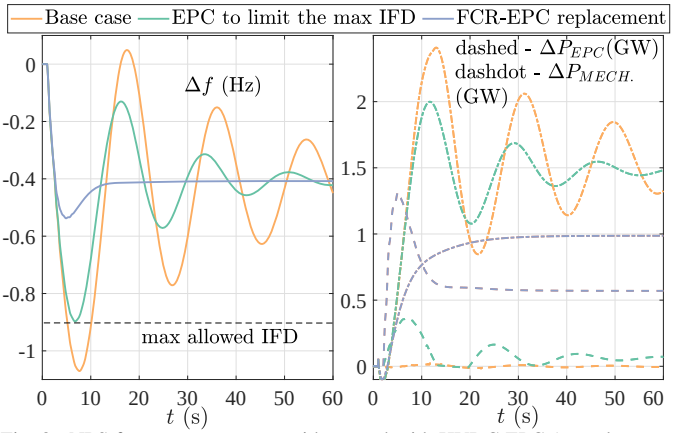

Fig. 8. NPS frequency response without and with HVDC EPC (complementing or replacing part of FCR-D)

The plots clearly show the frequency response improvement in terms of both maximum IFD and damping of the common mode of rotor oscillation. They also show the reduction of mechanical power output. This improvement comes as the cost of increased EPC reserves of 0, 373 and 1310 MW, respectively. These values are the peak EPC outputs in the right plots of Fig. 8 (dashed lines).

Finally, Fig. 9 shows how the maximum IFD, the generator FCR, the EPC reserve and the total reserves defined in (2) evolve with $\Delta\beta_g$. The results are given for two EPC activation frequencies, namely 49.6 and 49.8 Hz. They show that using the FCR-EPC replacement strategy given by Eq. (A.7), the maximum IFD is more improved when using the lower EPC activation frequency. In both cases, for increasing values of $\Delta\beta_g$, FCR decreases linearly, as shown with a dashed green line on the right plot of Fig. 9. On the other side, the EPC reserves increase, accounting for both $\Delta\beta_g$ and max IFD change. These observations can be also seen in (2). Due to this trade-off, the total reserves representing the sum of FCR and EPC slightly increase depending on the choice of the EPC

activation level.

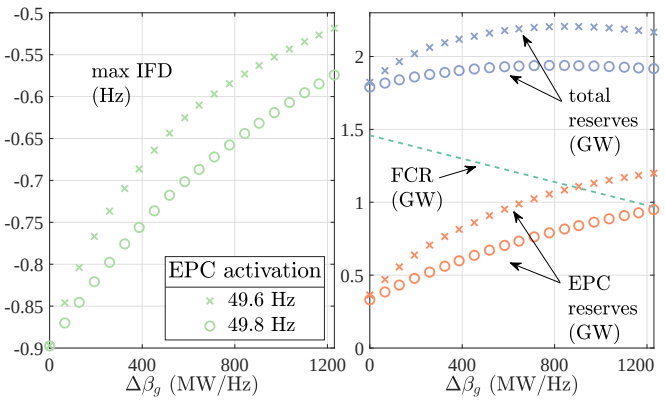

Fig. 9. Impact of FCR replacement ($-\Delta\beta_g$) by additional EPC reserves ($+\Delta\beta_h$)

Further interesting observations are shown in Appendix B related to the potential reserve cost savings and FCR-EPC replacement method.

C. Interaction between NSWPH and NPS

This section deals with NPS frequency support from the NSWPH, as well as the propagation of large disturbances from NSWPH to NPS. Two case studies are performed. In the first study, the dynamic behavior of the NPS and NSPWH systems is investigated in response to the dimensioning incident in NPS. In the second study, the outage of the HVDC link connecting NSWPH and The Netherlands is considered, in order to evaluate how large disturbances propagate from NPSWH to NPS. For the analyses, the active power flows between NSPWH and the interconnected onshore grids are mainly investigated.

The control of the active power flows between NSWPH and the onshore grids has been outlined in Section III. It relies on the active power control loops of the offshore AC/DC terminal converters. In the low-inertia option the latter operate in grid-following mode with frequency gains set to 3.5 pu, a value that allows the SCs to play their role of kinetic energy buffers while preventing too large deviations of their rotor speeds (and, hence, of frequency). In the zero-inertia option, the same converters operate in grid-forming mode with frequency droops set to 0.01 pu to ensure small-signal stability of the offshore system [42]. In both cases, the integral gain K_{hc} of the hub coordinator was set to 1.65 pu/s. The onshore AC/DC terminal converters control the DC voltages of their respective links.

1) Case study I - Dimensioning incident in NPS: The objective with this study is to investigate how NSWPH can support the NPS frequency, considering the same NPS dimensioning incident as in Sections V-A and V-B.

To this end, HVDC EPC has been assigned to the link between NSWPH and Norway (see Fig. 2), referred to as NSWPH-NO. The active power control loop of its offshore terminal is provided with a supplementary control receiving the onshore frequency error signal. The EPC gain was set to 22.2 pu. For comparison purposes, results are provided for the low-inertia design of NSPWH.

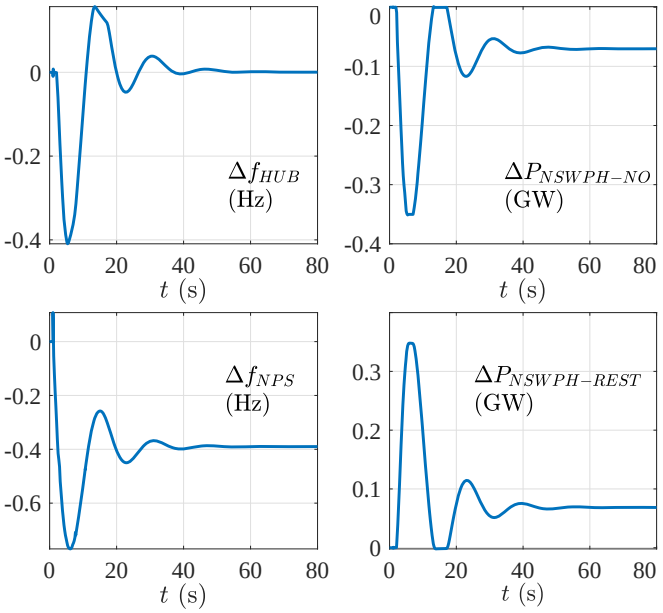

Fig. 10. Dimensioning incident in NPS with EPC on NSWPH-NO link and low-inertia option for NSWPH: evolution of frequencies and active power flows

Fig. 10 shows the NSWPH and NPS frequencies, the power flow in the NSWPH-NO link, and the sum of power flows in the other links connected to the NSWPH, in response to the dimensioning incident. At 2.1 s the NPS frequency drops below 49.6 Hz, activating EPC on the NSWPH-NO link. The power flow from NO to NSWPH is decreased to support the NPS frequency. As a consequence, the NSPWH frequency deviates. Considering that the frequencies of the NSWPH and NPS systems are coupled through the EPC on the NSWPH-NO link, the oscillations of the NSWPH frequency follow those of the NPS, through the power changes imposed by the terminal converter of that link.

Since, the offshore terminal converters of the other links participate in the control of the NSWPH frequency, as explained in Section III, their active power flows are adjusted in order to maintain the power balance in NSWPH. For an EPC gain of 22.2 pu, the maximum frequency deviation in the offshore system is 0.4 Hz. Larger deviations would be observed for larger EPC gains. Last but not least, due to the integral action of the hub coordinator, the NSWPH frequency deviation is zero at steady state.

2) Case Study II - Outage of the NSWPH-NL HVDC link: NSWPH is a system extension and, as such, it can be the source of additional disturbances. In this context, simulation results are provided pertaining to the outage of the HVDC link connecting NSWPH and The Netherlands (see Fig. 2), referred to as NSWPH-NL. With a pre-disturbance power flow of 1743 MW, the loss of that link significantly impacts the active power balance of the isolated, offshore AC system. The objective with this study is to validate how fast a disturbance is propagated to the interconnected onshore grid. For comparison purposes, results are provided for the zero- and low-inertia designs of NSWPH.

Figure 11 compares the low- and zero-inertia options in

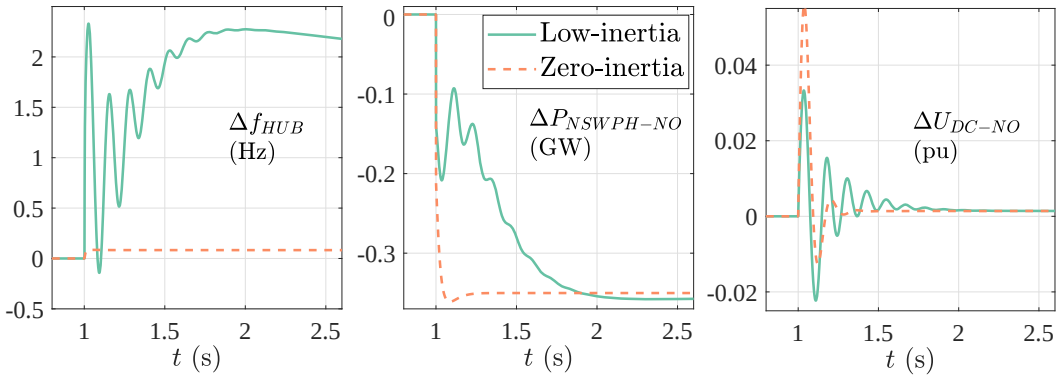

Fig. 11. Outage of the NSWPH-NL in the low- and zero-inertia configurations: frequency, active power, and DC voltage observed in the NSWPH-NO link.

terms of NSWPH and NPS frequencies, power flow in the NSWPH-NO link, and sum of power flows in the other links connected to the NSWPH.

In the low-inertia design, the kinetic energy storage in the SCs yields an active power adjustment of the offshore AC/DC converters with slower settling time. The rotor speeds and, hence, the NSWPH frequency, deviate quite significantly, with a maximum of 2.3 Hz. Although this deviation should be carefully taken into account when setting protections, no load is impacted in the offshore grid. Furthermore, the deviation could be made smaller by increasing the inertia of the rotating masses (using flywheels). The shown results correspond to a value of 5 s for the inertia constant H of the SCs.

In contrast, in the absence of offshore energy storage, the zero-inertia design results in an almost instantaneous response of the AC/DC converters operating in grid-forming mode. The NSWPH frequency reaches its post-disturbance value in a few milliseconds and deviates from the nominal value by 0.12 Hz only. This is to be expected from the respective frequency gains: 3.5 pu for the grid-following converters vs. 100 pu for the grid-forming ones.

The almost instantaneous response of the zero-inertia design is also easily seen from the HVDC link powers. They reach their post-disturbance values in some 0.2 s with a tiny overshoot. The rate of change of power is less abrupt in the low-inertia case, resulting in a slower propagation of the disturbance in the HVDC links and consequently in smaller maximum DC voltage deviation, as shown in Fig. 11.

VI. Conclusion

In this paper, a detailed model of the future Northern European AC/DC power system has been used to study its frequency response to large disturbances with and without EPC, respectively. The use of that model instead of the classical single-mass equivalent has been justified, the difference stemming from the load dependency on voltage.

Moreover, a plausible extension of the grid to the NSWPH has been considered as additional control means, considering either a low or a zero inertia option for its own control.

It has been shown that, if the current frequency control requirements are kept unchanged, it may not be possible to contain frequency within the acceptable frequency range after the most severe plant outage. It has been also shown that FCR-D alone may not be suitable to deal with this risk; additional reserves are needed.

The frequency deviation requirements can be satisfied by activating EPC on HVDC links. More precisely, the simulation results show that HVDC EPC can be used to either complement or replace the existing FCR, instead of conventional generating units. The control of HVDC links based on frequency droop significantly improves the IFD, due to the faster active power control of HVDC compared to hydro generation.

When investigating the interactions between the NSWPH and offshore grids, it was shown to which extent the hub can support the NPS frequency and how disturbances on the hub propagate to the aforementioned grids.

Appendix A

The content of this appendix is intended for supporting the mathematical definitions and derivations of Section VI.

After a power disturbance in the system, and a new SSFD of $\Delta f_{ss,g}$, there is a total power output of FCR units of $\Delta P_{ss,m}$— equal to FCR reserves $P_{res,\text{fcr}}$ for the largest power imbalance. From here, the total steady-state gain of FCR units in MW/Hz (or FCR regulating strengths) β_{g0} is defined as:

$$\beta_{g0} = \frac{\Delta P_{ss,m}}{\Delta f_{ss,g}}. \tag{A.3}$$

For the sake of simplicity all the frequency deviation inputs used in the derivations are considered as positive. Total EPC power output ΔP_{epc} is proportional to the frequency input of Δf_h through the EPC gain (in MW/Hz) constant β_h:

$$\Delta P_{\text{epc}} = \beta_h \Delta f_h. \tag{A.4}$$

This equation is assumed to be valid for both steady-state and transient responses due to the fast dynamics of the HVDC power response and well-damped system frequency. The EPC steady-state and maximum inputs are defined as $\Delta f_{ss,h}$ and $\Delta f_{\text{ifd},h}$, respectively. As previously mentioned, these inputs are different from the FCR due to different activation levels (f_g= 49.9 Hz and f_h =49.6 or 49.8 Hz in our tested cases). Unlike FCR, the maximum frequency deviation input $\Delta f_{\text{ifd},h}$ defines the EPC reserves as follows:

$$P_{res,\text{epc}} = \beta_h \Delta f_{\text{ifd},h}. \tag{A.5}$$

Properly defined β_{g0} (with at least 3625 MW/Hz) can keep the SSFD within the defined margin (49.5 Hz). However, to reduce the maximum IFD to be equal to the allowed value (49 Hz), additional EPC support is needed with β_{h0} value, meaning that:

$$(\beta_{go}, \beta_{h0}) \implies \text{max. allowed IFD \& SSFD} \tag{A.6}$$

Our method regarding the replacement of FCR reserves with additional EPC concerns that FCR gain decrease as $\beta_{g0} - \Delta\beta_g$ and EPC increase as $\beta_{h0} + \Delta\beta_h$, where $\Delta\beta_h$ is defined with (1), and it can be illustrated as:

$$(\beta_{go} - \Delta\beta_g, \beta_{h0} + \Delta\beta_h) \implies \text{less IFD \& the same SSFD} \tag{A.7}$$

It implies that there are no changes in total system regulating strengths (with taking into account different activation between FCR and EPC). Using this method, total reserves P_{res} are now defined as in (2).

Additionally, it is important clarifying that the values β_{g0}, β_{h0}, and $\Delta f_{\text{ifd},h}$ are obtained using dynamical simulations and take into account all the system properties.

Remarks: There are follwoing notable assumptions: i) Adding β_{h0} to β_{g0} decreases slightly SSFD which is neglected, ii) when we replace part of the reserves from FCR ($-\Delta\beta_g$) with additional EPC ($+\Delta\beta_h$) we assume that impact of loads and losses to SSFD will not change significantly, and iii) while providing EPC, HVDC links outputs do not reach their power limits.

Appendix B

This appendix provides some of the interesting insights of FCR-EPC reserve replacement related to the cost savings. Let the FCR and EPC reserves be penalized with the cost of c_g and c_h, respectively (c_g and c_h are given in \$/MW). In this study, it is assumed that c_g and c_h are constants. The total cost of reserves C_{res} can be written then as:

$$C_{res} = c_g P_{res,\text{fcr}} + c_h P_{res,\text{epc}}, \tag{B.8}$$

where $P_{res,\text{fcr}}$ and $P_{res,\text{epc}}$ are indicated in the right side of equation (2) as FCR and EPC reserves. It is of interest to assess the change of the cost benefits ΔC_{res} as a function of $\Delta\beta_g$, and if it gets lower than zero:

$$\Delta C_{res} = C_{res}|_{\text{new}} - C_{res}|_{(\beta_{g0}, \beta_{h0})} < 0. \tag{B.9}$$

Using the expressions in (2), applying mathematical manipulations, and introducing Δf_m as an improvement in the frequency nadir from the maximum allowed frequency deviation $\Delta f_{\text{ifd},h0}$ (referring to the difference in maximum IFD inputs between (A.6) and (A.7)), then the following is obtained:

$$\begin{aligned} \Delta C_{res} = c_h \Big(&- \Delta f_m (\beta_{h0} + \frac{\Delta f_{ss,g}}{\Delta f_{ss,h}} \Delta\beta_g) + \\ &+ \Delta f_{ss,g} \Delta\beta_g (\frac{\Delta f_{\text{ifd},h0}}{\Delta f_{ss,h}} - \frac{c_g}{c_h}) \Big). \end{aligned} \tag{B.10}$$

The cost function ΔC_{res} divided by constant c_h (the same sign is kept since $c_h > 0$) is illustrated in Fig.12 for two different EPC activation levels and three different cost rations between FCR and EPC: c_g/c_h =1.0, 1.5 and 2.0.

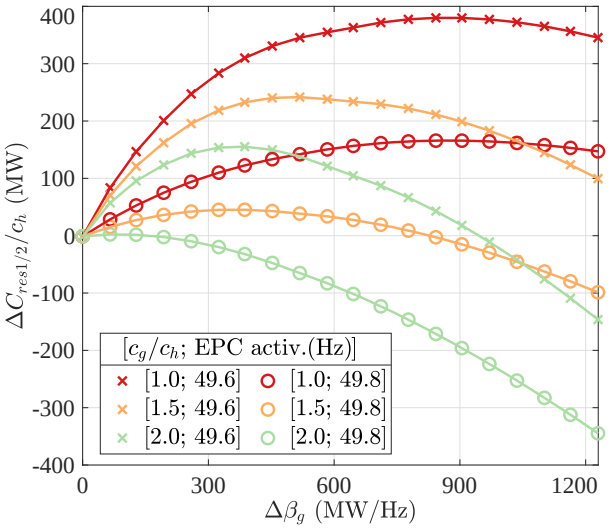

Fig. 12. Impact of FCR replacement ($-\Delta\beta_g$) by additional EPC reserves ($+\Delta\beta_h$) on cost function benefits depending on a ratio between FCR and EPC cost c_g/c_h and EPC activation level.

From here, it is concluded that, apart from obtaining a better frequency response with FCR-EPC replacement, there could also be financial benefits if FCR is more expensive than EPC. For higher values of c_g/c_h ratio there is specific $\Delta\beta_g$ for which benefits are obtained. If this value is too high, such as c_g/c_h=2 and EPC is activated from 49.8 Hz, then there are cost benefits for any value of $\Delta\beta_g$. The scenario where $c_g/c_h > 1$ might happen in the future operation of NPS, since there will be plenty of HVDC interconnection capacity and possible available headroom for the cheap EPC support. Also, if the EPC is activated sooner, the cost benefits can be achieved with less $\Delta\beta_g$ value.

References

[1] O. Dudurych and M. Conlon, "Impact of Reduced System Inertia as a Result of Higher Penetration Levels of Wind Generation," in *2014 49th Int. UPEC*, 2014, pp. 1–6.

[2] EirGrid and SONI, "RoCoF Alternative and Complementary Solutions Project," Tech. Rep., Mar. 2016.

[3] AEMO, "Future Power System Security Program (FPSSP) - Progress report," Tech. Rep., Mar. 2017.

[4] National Grid, "Operating a Low Inertia System - A System Operability Framework document," Tech. Rep., Feb. 2020.

[5] Nordic TSOs, "Challenges and Opportunities for the Nordic Power System," Tech. Rep., Aug. 2016.

[6] IRENA, "Renewable energy statistics 2020," Tech. Rep., Jul. 2020, ISBN: 978-92-9260-246-8, p. 28.

[7] WindEurope, "Wind energy in Europe: Scenarios for 2030," Tech. Rep., Sep 2017.

[8] C. George *et al.* (2019), Electricity interconnections with neighbouring countries - Second report of the Commission Expert Group on electricity interconnection targets. 10.2833/092722.

[9] Svenska kraftnät: 'Långsiktig marknadsanalys 2018 (Long-term market analysis 2018),' Tech. Rep., Jan. 2019.

[10] E. Ørum *et al.*, "Future System Inertia 2," European Network of Transmission System Operators for Electricity (ENTSO-E), Tech. Rep., Aug. 2018.

[11] E. Solvang, I. Sperstad, S. Jakobsen and K. Uhlen, "Dynamic simulation of simultaneous HVDC contingencies relevant for vulnerability assessment of the nordic power system," *IEEE Milan PowerTech*, June 2019, Milan, Italy.

[12] M. Kuivaniemi *et al.*, "New primary reserve requirements in the Nordic synchronous area – Designing the disturbance reserve," *Cigre 2018 Session*, Ref. C2-203_2018, Paris, 2018.

[13] A. Tosatto, M. Dijokas, T. Weckesser, S. Chatzivasileiadis, R. Eriksson, "Sharing Reserves through HVDC: Potential Cost Savings in the Nordic Countries", in *IET Gener. Transm. Distrib.*, Sep. 2020.

[14] D. Obradović, M. Ghandhari and R. Eriksson, "Assessment and Design of Frequency Containment Reserves with HVDC Interconnections," *2018 North American Power Symposium (NAPS)*, Fargo, ND, pp. 1-6, 2018.

[15] "Operational Limits and Conditions for Mutual Frequency support over HVDC", ENTSO-e Tech. Rep., 2021.

[16] O. Saborío-Romano, A. Bidadfar, J. N. Sakamuri, L. Zeni, Ö. Göksu and N. A. Cutululis, "Communication-Less Frequency Support From Offshore Wind Farms Connected to HVdc via Diode Rectifiers," *IEEE Trans. Sustain. Energy*, vol. 12, no. 1, pp. 441-450, Jan. 2021.

[17] P. Kou, D. Liang, Z. Wu, Q. Ze and L. Gao, "Frequency Support From a DC-Grid Offshore Wind Farm Connected Through an HVDC Link: A Communication-Free Approach," *IEEE Trans. Energy Convers.*, vol. 33, no. 3, pp. 1297-1310, Sept. 2018.

[18] I. Martínez Sanz, B. Chaudhuri and G. Strbac, "Inertial Response From Offshore Wind Farms Connected Through DC Grids," *IEEE Trans. Power Syst.*, vol. 30, no. 3, pp. 1518-1527, May 2015.

[19] T. M. Haileselassie and K. Uhlen, "Primary frequency control of remote grids connected by multi-terminal HVDC," *IEEE PES General Meeting*, 2010, pp. 1-6.

[20] M. N. Ambia, K. Meng, W. Xiao, A. Al-Durra and Z. Y. Dong, "Adaptive Droop Control of Multi-Terminal HVDC Network for Frequency Regulation and Power Sharing," *IEEE Trans. Power Syst.*, vol. 36, no. 1, pp. 566-578, Jan. 2021.

[21] N. R. Chaudhuri, R. Majumder and B. Chaudhuri, "System Frequency Support Through Multi-Terminal DC (MTDC) Grids," *IEEE Trans. Power Syst.*, vol. 28, no. 1, pp. 347-356, Feb. 2013.

[22] B. Hartmann, I. Vokony, and I. Taczi, "Effects of decreasing synchronous inertia on power system dynamics - Overview of recent experiences and marketisation of services," *Int. Trans. Electr. Energy Syst.*, vol. 29, no. 12, June 2019.

[23] ENTSO-E: "Fast Frequency Reserve – Solution to the Nordic inertia challenge," European Network of Transmission System Operators for Electricity (ENTSO-E), Tech. Rep., Dec. 2019.

[24] Y. Jiang, R. Pates and E. Mallada, "Dynamic Droop Control in Low-Inertia Power Systems," *IEEE Trans. Automat. Contr.*, vol. 66, no. 8, pp. 3518-3533, Aug. 2021.

[25] L. Papangelis, M.S. Debry, T. Prevost, P. Panciatici, and T. Van Cutsem, "Decentralized Model Predictive Control of Voltage Source Converters for AC Frequency containment," *Int. J. Electr. Power Energy Syst.*, vol. 98, pp. 342-349, 2018.

[26] B. K. Poolla, D. Groß and F. Dörfler, "Placement and Implementation of Grid-Forming and Grid-Following Virtual Inertia and Fast Frequency Response," *IEEE Trans. Power Syst.*, vol. 34, no. 4, pp. 3035-3046, July 2019.

[27] M. Ashabani and Y. A. I. Mohamed, "Novel Comprehensive Control Framework for Incorporating VSCs to Smart Power Grids Using Bidirectional Synchronous-VSC," *IEEE Trans. Power Syst.*, vol. 29, no. 2, pp. 943-957, Mar. 2014.

[28] D. Obradovic, M. Oluic, R. Eriksson and M. Ghandhari, "Supplementary Power Control of an HVDC System and its Impact on Electromechanical Dynamics," *IEEE Trans. Power Syst.*, vol. 36, no. 5, pp. 4599-4610, Sept. 2021.

[29] L. Harnerfors, N. Johansson and L. Zhang, "Impact on interarea modes of fast HVDC primary frequency control," *IEEE Trans. Power Syst.*, vol. 32, no. 2, pp. 1350-1358, Mar. 2017.

[30] European Commision, "Political Declaration on energy cooperation between the North Seas Countries," Jun. 2016.

[31] G. Misyris, T. Van Cutsem, J. Moller, M. Dijokas, O. Renom Estragues, B. Bastin, S. Chatzivasileadis, A. H. Nielsen, T. Weckesser, J. Ostergaard, F. Kryezi, "North Sea Wind Power Hub: System Configurations, Grid Implementation and Techno-economic Assessment", *Cigre e-Session 2020*, Paris, France, pp.1-15, Aug. 2020.

[32] P. Kundur, *Power system Stability and Control*, EPRI Power System Engineering Series, McGraw Hill, 1994.

[33] ENTSO-E: "Nordic Balancing Philosophy," European Network of Transmission System Operators for Electricity (ENTSO-E) Tech. Rep., Jun. 2016

[34] DIgSILENT, "PowerFactory 2018 - User Manual," Oct. 2018.

[35] M. Dijokas, D. Obradović, G. Misyris, T. Weckesser and T. Van Cutsem, Northern European AC/DC Power System model, GitHub repository, 2021. Available: https://github.com/thematt199310/NorthEuropeanAC-DCPowerSystem-Model/.

[36] "IEEE Guide for Synchronous Generator Modeling Practices and Parameter Verification with Applications in Power System Stability Analyses," in IEEE Std 1110-2019 (Revision of IEEE Std 1110-2002), pp.1-92, 2 Mar. 2020.

[37] E. Hillberg, "Development of improved aggregated load models for power system network planning in the Nordic power system Part 2: Method verification," *Cigre 2018 Session*, Ref. C4-310_2018, Paris, 2018.

[38] N. Vovos and CIGRE Working Group 14.02, "The CIGRE HVDC benchmark model - A new proposal with revised parameters," ELECTRA 157, p. 61-66, 1994.

[39] M. M. Belhaouane, J. Freytes, P. Rault, F. Colas and X. Guillaud, "Modeling and Analysis of Modular Multilevel Converters connected to Weak AC Grids," *2019 21st European Conference on Power Electronics and Applications (EPE '19 ECCE Europe)*, pp. P.1-P.11, 2019.

[40] The North Wind Power Hub Consortium, "The vision: The Hub-and-Spoke concept as modular infrastructure block to scale up fast", June 2019.

[41] M. Paolone, C.T. Gaunt, X. Guillaud, M. Liserre, A.P. Meliopoulos, A. Monti, T. Van Cutsem, V. Vittal, C. Vournas, Costas, "Fundamentals of Power Systems Modelling in the Presence of Converter-Interfaced Generation", *Proc. 21st Power System Computation Conference (PSCC)*, 2020.

[42] G. Misyris, S. Chatzivasileiadis and T. Weckesser, "Grid-forming converters: Sufficient conditions for RMS modeling," *Electr. Power Syst. Res.*, Volume 197, 2021, ISSN 0378-7796.

[43] G. Misyris, A. Tosatto, S. Chatzivasileiadis and T. Weckesser, "Zero-inertia Offshore Grids: N-1 Security and Active Power Sharing," *Submitted to IEEE Trans. Power Syst.*, 2020.

[44] T. Qoria, F. Gruson, F. Colas, G. Denis, T. Prevost and X. Guillaud, "Critical Clearing Time Determination and Enhancement of Grid-Forming Converters Embedding Virtual Impedance as Current Limitation Algorithm," *IEEE Trans. Emerg. Sel. Topics Power Electron.*, vol. 8, no. 2, pp. 1050-1061, June 2020.

[45] A. Tosatto, X. Martínez-Beseler, J. Østergaard, P. Pinson and S. Chatzivasileiadis, "North Sea Energy Islands: Impact on National Markets and Grids," *Submitted to Energy Policy*, 2021.

[46] M. Kuivaniemi, N. Modig and R. Eriksson, "FCR-D Design of Requirements," ENTSO-E Tech. Rep., July, 2017.

Danilo Obradović (S'18) received the B.Sc. and M.Sc. degrees in electrical engineering at the Department of Power Systems from the School of Electrical Engineering, University of Belgrade, Serbia, in 2016 and 2017, respectively. He obtained a Licentiate degree in electrical engineering at the Division of Electric Power and Energy Systems, KTH Royal Institute of Technology, Stockholm, Sweden, in 2020.

He is currently pursuing a Ph.D. degree with the KTH Royal Institute of Technology. His research interests include power system dynamics, stability and control, and HVDC systems.

Matas Dijokas (S'21) obtained his BSc. degree from Kaunas Technical University in 2016. In 2018 he obtained his MSc. degree in Electrical engineering from the Technical University of Denmark. Afterward, he continued as a researcher, and over 5 years he accumulated deep expertise in power system frequency stability and control, modeling of large power systems with high renewable energy source penetration, and HVDC systems. Currently, Matas pursue a career in industry sectors and works as a Modelling Expert at Ignitis Group.

Georgios S. Misyris (S'16) was born in Thessaloniki, Greece, in 1992. He received the Diploma in electrical and computer engineering from the Aristotle University of Thessaloniki, Thessaloniki, Greece and the Ph.D. degree from Denmark Technical University, Lyngby, Denmark in 2021. His research interests include power system modeling, control of AC and HVDC grids, machine learning applications for power systems and battery energy storage systems.

Tilman Weckesser (SM' 21) received his M.Sc. and Ph.D. degree from the Technical University of Denmark (DTU), Lyngby, Denmark, in 2011 and 2015, respectively. He was affiliated with the University of Liège, Belgium, as a postdoctoral researcher. From 2019 – 2022 he was a consultant at Danish Energy in the Grid technology department. Currently, he is affiliated with the Technical University of Denmark as Assistant Professor (tenure track). His research interests are in electric power system dynamics, stability, and integration of active distribution grids.

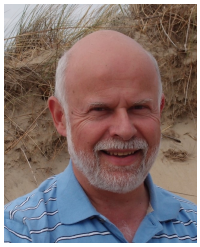

Thierry Van Cutsem (F' 05) received the M.Sc. and Ph.D. degrees from the University of Liège, Belgium, where he spent his career as a Research Director of the Fund for Scientific Research (FNRS) and an Adjunct Professor at the Dept. of Electrical Engineering and Computer Science. Being retired he is now a consultant/adviser. His research interests include power system dynamics, security, monitoring, control, and simulation. He collaborated with several TSOs in Europe and Canada. He served as Chair of the IEEE Power System Dynamic Performance Committee.